

## Probing singularities of Landau-gauge propagators with Padé approximants

Cristiane Yumi London,<sup>a,b,\*</sup> Diogo Boito,<sup>a</sup> Attilio Cucchieri<sup>a</sup> and Tereza Mendes<sup>a</sup>

<sup>a</sup>*Instituto de Física de São Carlos, Universidade de São Paulo,  
Caixa Postal 369, 13560-970 São Carlos, SP, Brazil*

<sup>b</sup>*Grup de Física Teòrica, Departament de Física, Universitat Autònoma de Barcelona, and Institut de Física d'Altes Energies (IFAE), The Barcelona Institute of Science and Technology (BIST), Campus UAB, E-08193 Bellaterra (Barcelona), Spain*

*E-mail: [cristiane.london@usp.br](mailto:cristiane.london@usp.br), [boito@ifsc.usp.br](mailto:boito@ifsc.usp.br), [attilio@ifsc.usp.br](mailto:attilio@ifsc.usp.br), [mendes@ifsc.usp.br](mailto:mendes@ifsc.usp.br)*

Padé approximants are employed in order to study the analytic structure of the four-dimensional SU(2) Landau-gauge gluon and ghost propagators in the infrared regime. The approximants, which are model independent, are used as fitting functions to lattice data for the propagators, carefully propagating uncertainties due to the fit procedure and taking into account all possible correlations. Applying this procedure systematically to the gluon-propagator data, we observe the presence of a pair of complex poles at  $p_{\text{pole}}^2 = (-0.37 \pm 0.05_{\text{stat}} \pm 0.08_{\text{sys}}) \pm i(0.66 \pm 0.03_{\text{stat}} \pm 0.02_{\text{sys}}) \text{ GeV}^2$ , where “stat” represents the statistical error and “sys” the systematic one. We also find a zero on the negative real axis of  $p^2$ , at  $p_{\text{zero}}^2 = (-2.9 \pm 0.4_{\text{stat}} \pm 0.9_{\text{sys}}) \text{ GeV}^2$ . We thus note that our procedure — which is based on a model-independent approach and includes careful error propagation — confirms the presence of a pair of complex poles in the gluon propagator, in agreement with previous works. For the ghost propagator, the Padés indicate the existence of the single pole at  $p^2 = 0$ , as expected. We also find evidence of a branch cut on the negative real axis. Through the use of the so-called D-Log Padé method, which is designed to approximate functions with cuts, we corroborate the existence of this cut for the ghost propagator.

*The 39th International Symposium on Lattice Field Theory,  
8th-13th August, 2022,  
Rheinische Friedrich-Wilhelms-Universität Bonn, Bonn, Germany*

---

\*Speaker

## 1. Introduction

Quantum chromodynamics (QCD), which is based on SU(3) Yang-Mills theory, describes the strong interactions involving quarks and gluons. One of its fundamental properties is color confinement, which states that no color-charged particles can be found in isolation. Indeed, up to now, no free quarks or gluons were observed in nature and hadronic states are all colorless. Confinement in QCD is related to the fact that the strong coupling,  $\alpha_s$ , runs with the energy, as predicted by the QCD  $\beta$ -function; in particular, in the usual (perturbative)  $\overline{\text{MS}}$  scheme,  $\alpha_s$  assumes large values at low momenta, i.e. in the infrared (IR) region, eventually diverging at the Landau pole. A complete theoretical explanation of color confinement is, however, still lacking. As a first step in this direction, one can try to understand the behavior of gluon and ghost propagators, which are the theory's fundamental degrees of freedom, in the IR limit, i.e. going beyond the validity of perturbative QCD.

Several theoretical frameworks were proposed to explain the color confinement mechanism (in Landau gauge), such as the Gribov-Zwanziger scenario [1, 2] and the scaling solution of Dyson-Schwinger equations [3], to name only two of them. Both descriptions — in their original formulations — predicted that the gluon propagator vanishes at zero momentum and the ghost propagator has an enhanced singularity, i.e. it is more singular than  $1/p^2$  in the IR limit. These properties were verified with lattice numerical simulations, using large lattice volumes, in 2 space-time dimensions [4, 5]. On the contrary, in 3 and in 4 dimensions [4–7], lattice data showed that the ghost propagator,  $G(p^2)$ , is not enhanced, i.e.  $G(p^2 \approx 0) \sim 1/p^2$ , and that the gluon propagator does not go to zero at the origin. These results for the propagators in the IR regime motivated novel theoretical models that are in accordance with lattice simulations, such as the decoupling solution of Dyson-Schwinger equations [8, 9], the Refined Gribov-Zwanziger scenario [10–12] and the Curci-Ferrari model [13, 14].

Here, we report some of the results recently presented in Ref. [15], to which we refer for further details. The aim of our work is to study — in a model-independent way — the analytic structure of the four-dimensional SU(2) (quenched) Landau-gauge gluon and ghost propagators in the IR regime, by using rational approximants as fitting functions to the data from Refs. [5, 6, 16]. We note that rational approximants were recently applied by Falcão, Oliveira and Silva [17, 18] to analyze the Landau-gauge gluon and ghost propagators in the SU(3) case. We stress, however, that in Refs. [17, 18] the issues related to error propagation, and in particular the uncertainties arising from the fit procedure, are not fully discussed. In this work we propagated all the errors, considering off-diagonal correlations when necessary. As shown in Ref. [15], this limits considerably the number of parameters that can be determined from our fits.

## 2. Padé Approximants

The main type of rational approximants that we will employ as fitting functions are the standard Padé approximants (PAs). We recall that a PA  $P_N^M(z)$  is a ratio of two polynomials of orders  $M$  and  $N$  [19, 20], i.e.,

$$P_N^M(z) = \frac{Q_M(z)}{R_N(z)} = \frac{a_0 + a_1 z + a_2 z^2 + \cdots + a_M z^M}{1 + b_1 z + b_2 z^2 + \cdots + b_N z^N}, \quad (1)$$

where we employed  $b_0 = 1$  without loss of generality. The canonical method of applying PAs is to approximate a function  $f(z)$  whose Taylor series is known. The Padé coefficients are then obtained through a matching to the Taylor-series coefficients of  $f(z)$  up to order  $N + M$ , upon the expansion of the Padé. Thus, the PA will reproduce the first  $N + M + 1$  Taylor coefficients of the function  $f(z)$ .

The most prominent advantage of employing PAs is that they allow for a systematic and model-independent analysis. Moreover, which is especially relevant to our work, they can reproduce analytic features of the function they are approximating, such as poles, residues and zeros. In addition, in some cases, the use of these approximants is validated by convergence theorems. The most important one for this work is Pommerenke's theorem, which states that PAs of the sequence  $P_N^{N+k}(z)$ , for fixed  $k$ , applied to a meromorphic function  $f(z)$ , converges to  $f(z)$  for  $N \rightarrow \infty$  [19, 20]. On the other hand, this theorem predicts that the Padé can have extraneous poles, which cannot be identified as singularities of the original function and move away when the order of the PA is increased. There are also spurious poles that can appear close to zeros, which are the *defects* or *Froissart doublets* [19–21] — these defects are of transient nature and should also disappear for PAs of higher order. It is important to stress that approximants with such defects can still be employed to study the considered function, away from these singularities.

In this work, we are going to use the Padé approximants as fitting functions to data, which departs from the standard Padé theory and is not supported by convergence theorems. However, experience shows that this approach is rather powerful and that its application to similar particle-physics problems, such as the extraction of resonance pole positions, is very successful [22–28]. We also recall that the gluon and ghost propagators are expected to have branch cuts in the complex plane and that, even though there are no general theorems for Padés applied to functions with cuts, it is observed that the approximants mimic the branch cut of the function by accumulating interleaved poles and zeros along the cut [19–21, 29]. A classic example in this context is the approximation of the function  $\log(z)$  by PAs.

### 3. Results

The lattice data fitted in this work have been previously presented in Refs. [5, 6, 16] where more technical details can be found. (See also Ref. [15].) In particular, we use the data from a (symmetric) lattice with volume  $V = n^4 = 128^4$ . The lattice parameter was taken to be  $\beta = 2.2$ , which leads to a lattice spacing  $a$  of approximately 0.210 fm, considering  $\sigma^{1/2} = 0.44$  GeV for the string tension [30]. Hence, the physical lattice volume is about  $(27 \text{ fm})^4$ , which can be essentially considered as infinite volume, and the lowest non-zero physical momentum allowed is  $p_{min} = 2a^{-1} \sin(\pi/n) \sim 46$  MeV.

The ghost-propagator data are considered in terms of the unimproved lattice momenta  $p^2 = \sum_{\mu} p_{\mu}^2$ , where  $p_{\mu} = 2 \sin(\pi \hat{p}_{\mu}/n)$  and  $\hat{p}_{\mu} = 0, 1, \dots, n-1$ . On the other hand, the gluon propagator  $D(p^2)$  is given in terms [31] of the improved momenta  $p^2 = \sum_{\mu} p_{\mu}^2 + \frac{1}{12} \sum_{\mu} p_{\mu}^4$ , for the sake of reducing the effects due to rotational-symmetry breaking, which are stronger at large momenta. Thus, this definition mostly affects the values of momenta outside the IR limit.

As shown in Ref. [15], the perturbative behavior of the gluon propagator sets in around 2.0 GeV; at the same time, the ghost-propagator data are essentially perturbative for momenta higher than 1.5 GeV. Hence, in our work we focus the Padé analysis mostly in the IR region.

### 3.1 Gluon propagator

We start by employing the Padé approximants as fitting functions to the four-dimensional SU(2) Landau-gauge gluon propagator data. The fit parameters are obtained through a  $\chi^2$  minimization, taking into account off-diagonal correlations when necessary. The fit uncertainties are calculated using four different methods: Hessian matrix, Monte Carlo error propagation,  $\Delta\chi^2$  variation and linear error propagation. We checked that results obtained with these four methods are in good agreement. The errors presented in this work were calculated using the Hessian matrix. As for the fit quality, it is judged by the minimum  $\chi^2$ , divided by the degrees of freedom (dof), and by the associated  $p$ -value. We stress that we limited the number of fit parameters to 7, because for Padés with higher order the statistical uncertainty grows considerably and the fit is not meaningful anymore. Also, the fits are performed in the region of  $\sqrt{p^2} < 2.4$  GeV, and we have verified that the correlation between the data points is negligible, so that it can be disregarded in the calculations.

The following Padé sequences were used to fit the lattice data:  $P_k^k(p^2)$ ,  $P_{k+1}^{k+1}(p^2)$ ,  $P_{k+1}^k(p^2)$  and  $P_{k+2}^k(p^2)$ . The PAs that pass all reliability tests,<sup>1</sup> together with the lattice data, are presented in Fig. 1a, where the white region is the fit window. Note that, except for  $P_2^3(p^2)$ , all the approximants follow the expected behavior of the propagator in the ultraviolet region. The behavior at high energies of  $P_2^3(p^2)$  can be explained by the fact that this Padé goes as  $a_4 p^2$  for large  $p^2$ , with  $a_4 > 0$  (albeit small). Due to the bad behavior of this PA, we did not use it in our final estimates.

The pole position for each approximant is shown in Fig. 1b and one can notice that the PAs have a consistent pair of complex poles. Our final value is obtained as follows: the central value is the average of all the Padés results, the statistical uncertainty is the largest one from the PAs, and the systematic error is half the maximum spread between results from two different PAs. Employing this procedure we find that the final position for the complex poles is

$$p_{\text{pole}}^2 = [(-0.37 \pm 0.05_{\text{stat}} \pm 0.08_{\text{sys}}) \pm i(0.66 \pm 0.03_{\text{stat}} \pm 0.02_{\text{sys}})] \text{ GeV}^2, \quad (2)$$

where the first error is statistical and the second systematic. This final value, which is indicated in gray in Fig. 1b (with the errors added in quadrature), is in agreement with other results available in the literature [5, 17, 18, 32]. Thus, the Padés clearly favor a pair of complex poles, with an imaginary part inconsistent with zero, for the Landau-gauge gluon propagator.

Another noticeable feature in all the PAs of Fig. 1a is the presence of a zero on the negative real axis of  $p^2$ . Applying the same method used for the pole, we obtain the result

$$p_{\text{zero}}^2 = (-2.9 \pm 0.4_{\text{stat}} \pm 0.9_{\text{sys}}) \text{ GeV}^2, \quad (3)$$

which is shown in Fig. 1c together with the zeros of the considered approximants.

### 3.2 Ghost propagator

We now turn to applying the Padé analysis to the Landau-gauge ghost propagator. The method is mostly the same used for the gluon propagator but, in this case, the correlation between the data points is significant, reaching up to 0.75 in non-diagonal entries. It is known that fits to strongly

<sup>1</sup>See Ref. [15] for more details.

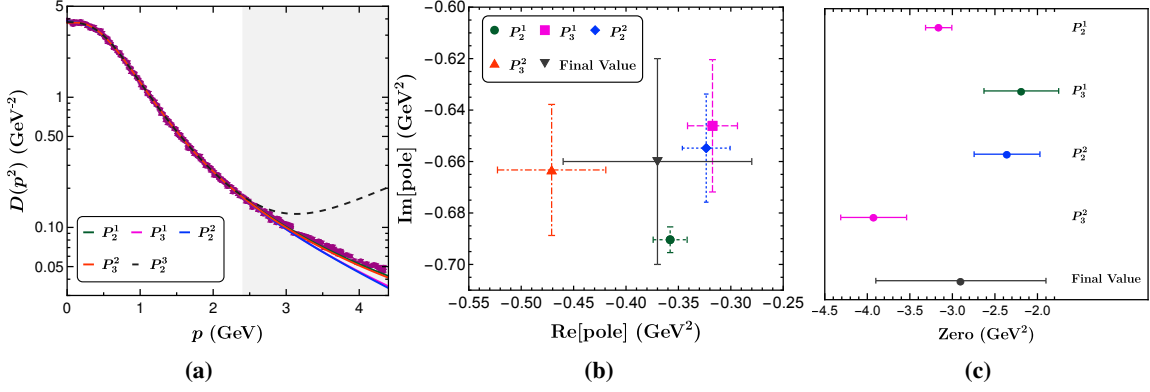


**Figure 1:** Padé approximants fitted to the Landau-gauge gluon-propagator data and used to determine the final results for poles and zeros. In (a) we show the comparison of the PAs (used to determine the final results) and the lattice data; the shaded region is not included in the fits. In (b), respectively (c), we present the poles, respectively the zeros, of each PA. In both cases we show our final prediction in gray.

correlated data are problematic, since the covariance matrix has small eigenvalues, which makes it hard to invert numerically. What is more, the small eigenvalues generate huge numbers in the inverse matrix. This engenders large fluctuations in the  $\chi^2$  values, which are not statistically meaningful, leading to biased [33] or unreliable [34] results. In order to avoid this problem, we will employ the so-called *diagonal fits* [34]. In this procedure, only the diagonal covariance matrix is used to determine the fit parameters; the corresponding fit quality is denoted here as  $Q^2$ . All correlations are then included in the error propagation according to the method explained in Ref. [34]. Let us stress that, since the diagonal covariance matrix is used, the fit quality cannot be judged in absolute terms by the value of  $Q^2/\text{dof}$ .

By employing Padé approximants to fit the lattice data of the ghost propagator, it turns out that all the fit parameters of the PAs are extremely large, of the order of  $O(10^{10})$  or higher. This is caused by a pole very close to the origin, as can be understood from Eq. (1). We also verify that this feature persists when considering different Padé approximants, indicating that this pole is indeed physical. For the sake of exploring additional analytical structures of the ghost propagator, we then impose this pole at the origin, through the so-called partial Padé approximants (PPAs) [19, 20], which, in this case, are expressed as

$$\mathbb{P}_N^M(p^2) = \frac{Q_M(p^2)}{R_N(p^2) p^2}, \quad (4)$$

where  $Q_M(p^2)$  and  $R_N(p^2)$  are defined as before.

The fits were performed in the region  $\sqrt{p^2} \leq 3.12$  GeV to avoid the appearance of Froissart doublets (in some PPAs) in the considered range of momenta, which can spoil the extrapolation of the fit results beyond the fit window. Indeed, as said above, these defects may appear, but the approximants can still be used away from these singularities. We applied partial Padés of the sequences  $\mathbb{P}_k^k(p^2)$ ,  $\mathbb{P}_{k+1}^k(p^2)$ ,  $\mathbb{P}_{k+2}^k(p^2)$  and  $\mathbb{P}_k^{k+1}(p^2)$  to fit the ghost-propagator data. As before, the number of parameters of the PPAs that can be used to fit the data is limited by the quality of the data. In particular, in this case, partial Padés up to order 8 can be used. The resulting PPAs and the

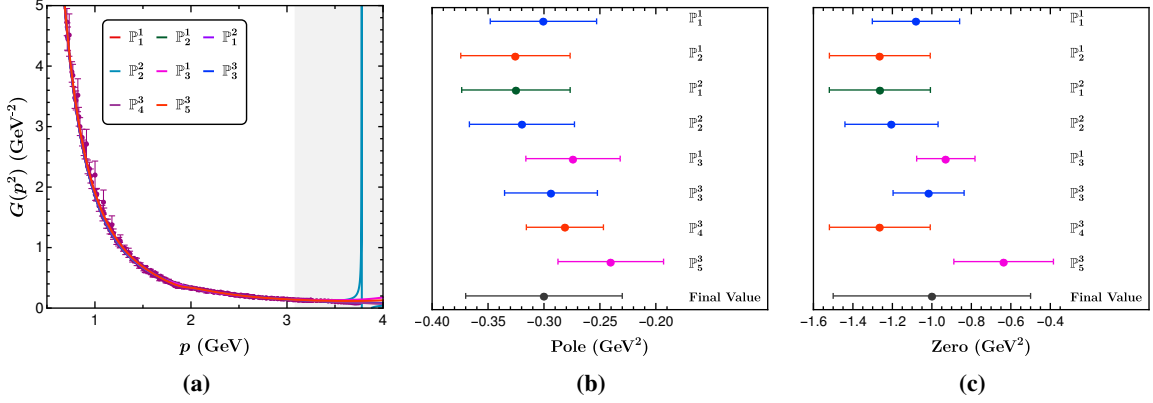


**Figure 2:** Partial Padé approximants fitted to the Landau-gauge ghost-propagator lattice data used to determine our final results for poles and zeros. In (a) we show the PPAs and the lattice data; the shaded region is not included in the fits. In (b), respectively (c), we present the poles, respectively the zeros, of each PPA. In both cases, our final values are shown in gray at the bottom of each plot. We recall that a pole (at about  $p^2 = -0.30 \text{ GeV}^2$ ) followed by a zero (at about  $p^2 = -1.0 \text{ GeV}^2$ ) points towards the presence of a branch cut along the negative real axis of  $p^2$ .

lattice data for the ghost propagator are shown in Fig. 2a, where the gray region is not considered in the fit. We note that  $\mathbb{P}_2^2(p^2)$  also has a pole on the positive real axis, which is almost cancelled by a near-by zero. This singularity is a Froissart doublet and is a transient artifact of the PPA.

The Padés also show a pole and a zero on the negative real axis of  $p^2$ , which suggests a cut for the ghost propagator, considering that, as we already stressed above, the Padés emulate a cut by accumulating interleaved poles and zeros. Moreover, even though the uncertainties in the position of the poles and zeros of PPAs of higher orders are large, it is possible to see that their central values also present this pattern. This corroborates the existence of a cut on the negative real axis.

The pole of each partial Padé that passes all reliability tests are shown in Fig. 2b. From these results we can determine our final estimate, which is calculated by the same procedure employed in the gluon-propagator analysis. This yields

$$p_{\text{pole}}^2 = (-0.30 \pm 0.05_{\text{stat}} \pm 0.05_{\text{sys}}) \text{ GeV}^2. \quad (5)$$

In addition, a zero is located at

$$p_{\text{zero}}^2 = (-1.0 \pm 0.3_{\text{stat}} \pm 0.4_{\text{sys}}) \text{ GeV}^2. \quad (6)$$

The zeros of the PPAs together with our final value are shown in Fig. 2c. As mentioned before, the appearance of interleaved pole and zero can be an indication of a cut on the ghost propagator.

For the sake of better analyzing the existence of a cut on the negative real axis, we also used the so-called D-Log Padé approximants [19, 20]. They are a suitable alternative for functions with branch cuts because, instead of working with the original function  $f(z)$ , which has a cut, one tries to approximate a new function  $F(z)$ , which only has simple poles, and then unfold the procedure. In particular, let us assume that the function we are interested in is given by [19, 20]  $f(z) = A(z) \frac{1}{(\mu-z)^\gamma} + B(z)$ , where  $A(z)$  and  $B(z)$  have a simple structure and are analytic at

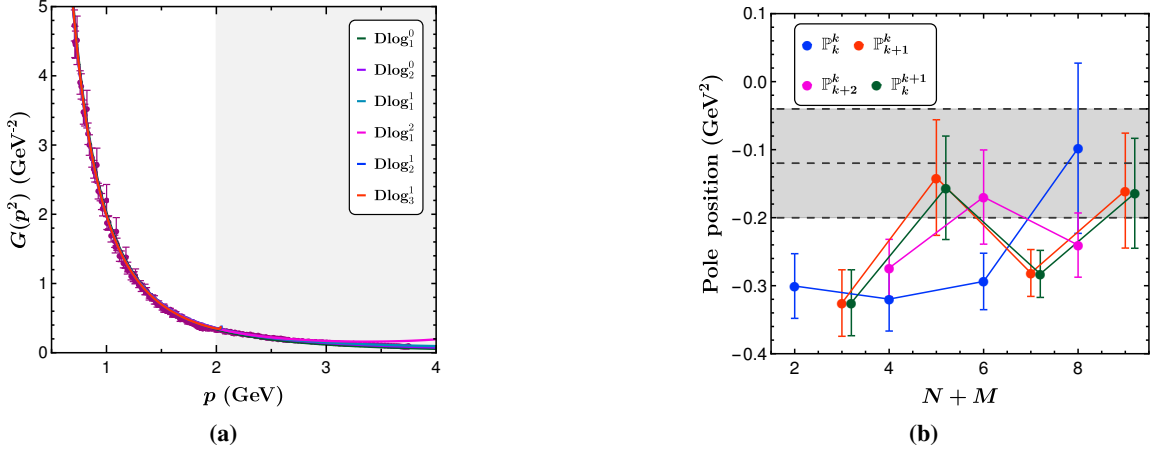


**Figure 3:** (a) Lattice data for the ghost propagator and the D-Log Padés, built from the first-order numerical derivative of the logarithm of the data. The shaded region is excluded from the fit. (b) Comparison of the largest (real and nonzero) pole position — from four different partial Padés sequences  $\mathbb{P}_N^M(p^2)$  — with the branch-point position  $p_c$  obtained from the D-Log Padés [see Eq. (8)] shown as the gray band.

$z = \mu$ , and where  $\gamma$  can be any real number. We then construct a new function defined as [19, 20]  $F(z) = \frac{d}{dz} \ln f(z) \approx \frac{\gamma}{(\mu-z)}$ . Thus, the branch point  $\mu$  of  $f(z)$  turns into a simple pole in  $F(z)$ , whose residue is equal to  $\gamma$ . Hence, by unfolding the procedure, the D-Log Padé  $\text{Dlog}_N^M(z)$  of  $f(z)$  is given by [19, 20]

$$\text{Dlog}_N^M(z) = f_{\text{norm}}(0) \exp \left\{ \int dz' \bar{P}_N^M(z') \right\}, \quad (7)$$

where the Padé  $\bar{P}_N^M(z')$  is applied to the function  $F(z)$  and the constant  $f_{\text{norm}}(0)$  has to be adjusted in order to reproduce the function at  $z = 0$ , since the constant (zeroth-order) term in the Taylor expansion of  $f(z)$  is lost due to the derivative.

Clearly, in order to apply the D-log Padés to the ghost propagator  $G(p^2)$ , we need lattice data for the function  $F(p^2)$ , which is the derivative of the logarithm of  $G(p^2)$ . This can be accomplished by first taking the logarithm of the data and then calculating the derivative, through finite differences. However, the standard formulas for the derivative require equally spaced data points, a property not satisfied by the ghost-propagator data. Hence, to address this problem, the logarithm of the lattice data has been linearly interpolated, to generate data points with a fixed separation of  $\Delta p^2 = 0.035 \text{ GeV}^2$ ; later, the derivative at a given point is determined through the usual first-order formula. Of course, this method introduces correlations between the data points, which were thoroughly calculated and propagated. We note that, after applying this procedure to the ghost-propagator data, the data points have large uncertainties (in some cases larger than 100%) with considerable statistical fluctuations.

For the D-Log Padés, the region chosen for the fit is  $\sqrt{p^2} \leq 2 \text{ GeV}$ , since the errors and fluctuations are quite large for higher momenta; moreover, the data around  $\sqrt{p^2} = 2 \text{ GeV}$  are already in the perturbative region (see Fig. 10a in Ref. [15]). We first apply the Padés  $\bar{P}_N^M(p^2)$  as fitting functions to the prepared data, again employing the diagonal-fit method due to the large correlation between the points. Afterwards, Eq. (7) is used to build the D-Log Padés belonging to the



sequences:  $\text{Dlog}_k^k(p^2)$ ,  $\text{Dlog}_{k+1}^k(p^2)$ ,  $\text{Dlog}_{k+2}^k(p^2)$  and  $\text{Dlog}_k^{k+1}(p^2)$ . Due to the large uncertainties and fluctuations of the data points, the maximum number of parameters was set to five. The D-log-Padé results are reported in Fig. 3a, together with the lattice data (in purple). The fits have been performed considering only the white region. It is possible to see a good agreement with the data, even outside the fit window. Moreover, every approximant of Fig. 3a has a singularity of the type  $(p_c - p^2)^{-\gamma}$ , where the branch point  $p_c$  is always located on the negative real axis, not too far from the pole determined by the partial Padés [see Eq. (5)], and the multiplicity  $\gamma$  is not compatible with one, which indicates that  $p_c$  is not a simple pole. Using these results, our final estimate for the branch-point position is

$$p_c^2 = (-0.12 \pm 0.08_{\text{stat}} \pm 0.02_{\text{sys}}) \text{ GeV}^2 . \quad (8)$$

It is important to emphasize that our systematic uncertainty for  $p_c$  may be underestimated, due to the fact that the evaluation of the numerical derivative introduces an additional source of error. This result, together with the exponent  $\gamma$  not being compatible with one, reinforces that the pole and zero of the PPAs are a manifestation of a cut on the negative real axis.

Finally, let us compare the branch point from the D-log Padés with the pole prediction of the partial Padés. We recall that, if the cut at negative  $p^2$  does exist, the largest (negative) pole of the PPAs should indicate the position of the branch point. In Fig. 3b the gray band corresponds to the (above) branch point predicted by the D-log PAs; we also show the largest non-zero pole position for different PPAs. As one can notice, the central values of the pole are in better agreement with  $p_c$  for higher-order PPAs. Also, the final results obtained for the branch point, Eq. (8), and for the pole extracted from the PPAs, Eq. (5), are compatible within  $1.7 \sigma$ . Thus, these results are in good agreement and corroborate the existence of a cut on the negative real axis for the ghost propagator.

## 4. Conclusions

In this work we applied a systematic and model-independent method to study the analytic structure of the IR Landau-gauge gluon and ghost propagators, by using rational approximants. In particular, Padé approximants, partial Padé approximants and also D-log Padé approximants were employed as fitting functions to four-dimensional SU(2) lattice data [5, 6, 16] of both propagators. We stress that Refs. [17, 18] also applied Padé approximants to fit SU(3) lattice propagators and our main conclusions are in agreement with their results. Notice, however, that in our work the errors were carefully propagated, considering all the correlations. In addition, we also estimated the systematic uncertainty of the employed method and explored other types of approximants: the partial Padés and the D-Log Padés.

For the gluon propagator, the Padé approximants presented evidence of a pair of complex poles located at  $p_{\text{pole}}^2 = [(-0.37 \pm 0.09) \pm i(0.66 \pm 0.04)] \text{ GeV}^2$ , where the errors are added in quadrature. The PAs also indicated a zero on the negative real axis at  $p_{\text{zero}}^2 = (-2.9 \pm 1.0) \text{ GeV}^2$ .

In the ghost-propagator case, the Padés clearly show the existence of a pole at the origin. We then imposed this information by using the so-called partial Padés to fit the ghost-propagator data. These fits indicated the presence of a pole, followed by a zero, on the negative real axis. Higher-order PPAs also had additional interleaved poles and zeros along the negative real axis, further suggesting the existence of a cut. In order to investigate this result, we employed D-Log



Padés and found a cut with branch point at  $p_c^2 = (-0.12 \pm 0.08) \text{ GeV}^2$ . This value is compatible with the pole obtained using partial Padés, which is another corroboration for the existence of a cut on the negative real axis for the ghost propagator.

## 5. Acknowledgements

DB's work was supported by the São Paulo Research Foundation (FAPESP) grant No. 2021/06756-6 and CNPq grant No. 308979/2021-4. AC and TM acknowledge partial support from FAPESP and CNPq. The work of CYL was financed by FAPESP grants No. 2020/15532-1 and No. 2022/02328-2 and CNPq grant No. 140497/2021-8.

## References

- [1] V. N. Gribov, Nucl. Phys. B **139**, 1 (1978).
- [2] N. Vandersickel and D. Zwanziger, Phys. Rept. **520**, 175-251 (2012), [[1202.1491](#)].
- [3] R. Alkofer and L. von Smekal, Phys. Rept. **353**, 281 (2001), [[hep-ph/0007355](#)].
- [4] A. Cucchieri and T. Mendes, Phys. Rev. Lett. **100**, 241601 (2008), [[0712.3517](#)]; Phys. Rev. D **78**, 094503 (2008), [[0804.2371](#)].
- [5] A. Cucchieri, D. Dudal, T. Mendes and N. Vandersickel, Phys. Rev. D **85**, 094513 (2012), [[1111.2327](#)]; Phys. Rev. D **93**, no.9, 094513 (2016), [[1602.01646](#)].
- [6] A. Cucchieri and T. Mendes, PoS **LATTICE2007**, 297 (2007), [[0710.0412](#)].
- [7] I. L. Bogolubsky, E. M. Ilgenfritz, M. Muller-Preussker and A. Sternbeck, Phys. Lett. B **676**, 69-73 (2009), [[0901.0736](#)].
- [8] A. C. Aguilar, D. Binosi and J. Papavassiliou, Phys. Rev. D **78**, 025010 (2008), [[0802.1870](#)].
- [9] P. Boucaud, J. P. Leroy, A. Le Yaouanc, J. Micheli, O. Pene and J. Rodriguez-Quintero, JHEP **06**, 099 (2008), [[0803.2161](#)].
- [10] D. Dudal, S. P. Sorella, N. Vandersickel and H. Verschelde, Phys. Rev. D **77**, 071501 (2008), [[0711.4496](#)]; Phys. Lett. B **680**, 377-383 (2009), [[0808.3379](#)].
- [11] D. Dudal, J. A. Gracey, S. P. Sorella, N. Vandersickel and H. Verschelde, Phys. Rev. D **78**, 065047 (2008), [[0806.4348](#)]; Phys. Rev. D **78**, 125012 (2008), [[0808.0893](#)].
- [12] D. Dudal, S. P. Sorella and N. Vandersickel, Phys. Rev. D **84**, 065039 (2011), [[1105.3371](#)].
- [13] M. Tissier and N. Wschebor, Phys. Rev. D **82** (2010), 101701, [[1004.1607](#)]; Phys. Rev. D **84** (2011), 045018, [[1105.2475](#)].
- [14] M. Pelaez, M. Tissier and N. Wschebor, Phys. Rev. D **88** (2013), 125003, [[1310.2594](#)].
- [15] D. Boito, A. Cucchieri, C. Y. London and T. Mendes, [[2210.10490](#)].

- [16] A. Cucchieri and T. Mendes, PoS **QCD-TNT09**, 026 (2009), [[1001.2584](#)].
- [17] A. F. Falcão, O. Oliveira and P. J. Silva, Phys. Rev. D **102**, no.11, 114518 (2020), [[2008.02614](#)].
- [18] O. Oliveira, A. F. Falcão and P. J. Silva, PoS **LATTICE2021**, 457 (2022), [[2111.04320](#)].
- [19] G. A. Baker Jr and P. Graves-Morris, **Padé approximants**, Cambridge University Press, Vol. 59, 1996.
- [20] G. A. Baker Jr *et al*, **Essentials of Padé approximants**, Elsevier, 1975.
- [21] P. Masjuan Queralt, [[1005.5683](#)].
- [22] P. Masjuan, S. Peris and J. J. Sanz-Cillero, Phys. Rev. D **78**, 074028 (2008), [[0807.4893](#)].
- [23] P. Masjuan, Phys. Rev. D **86**, 094021 (2012), [[1206.2549](#)].
- [24] P. Masjuan and J. J. Sanz-Cillero, Eur. Phys. J. C **73**, 2594 (2013), [[1306.6308](#)].
- [25] R. Escribano, P. Masjuan and P. Sanchez-Puertas, Phys. Rev. D **89**, no.3, 034014 (2014), [[1307.2061](#)].
- [26] P. Masjuan and P. Sanchez-Puertas, JHEP **08**, 108 (2016), [[1512.09292](#)]; Phys. Rev. D **95**, no.5, 054026 (2017), [[1701.05829](#)].
- [27] I. Caprini, P. Masjuan, J. Ruiz de Elvira and J. J. Sanz-Cillero, Phys. Rev. D **93**, no.7, 076004 (2016), [[1602.02062](#)].
- [28] L. Von Detten, F. Noël, C. Hanhart, M. Hoferichter and B. Kubis, Eur. Phys. J. C **81**, no.5, 420 (2021), [[2103.01966](#)].
- [29] O. Costin and G. V. Dunne, Eur. Phys. J. ST **230**, no.12-13, 2679-2690 (2021), [[2108.01145](#)].
- [30] J. C. R. Bloch, A. Cucchieri, K. Langfeld and T. Mendes, Nucl. Phys. B **687**, 76-100 (2004), [[hep-lat/0312036](#)].
- [31] J. P. Ma, Mod. Phys. Lett. A **15**, 229-244 (2000), [[hep-lat/9903009](#)].
- [32] D. Dudal, O. Oliveira and P. J. Silva, Annals Phys. **397**, 351-364 (2018), [[1803.02281](#)].
- [33] G. D'Agostini, Nucl. Instrum. Meth. A **346**, 306-311 (1994).
- [34] D. Boito, O. Cata, M. Golterman, M. Jamin, K. Maltman, J. Osborne and S. Peris, Phys. Rev. D **84**, 113006 (2011), [[1110.1127](#)].